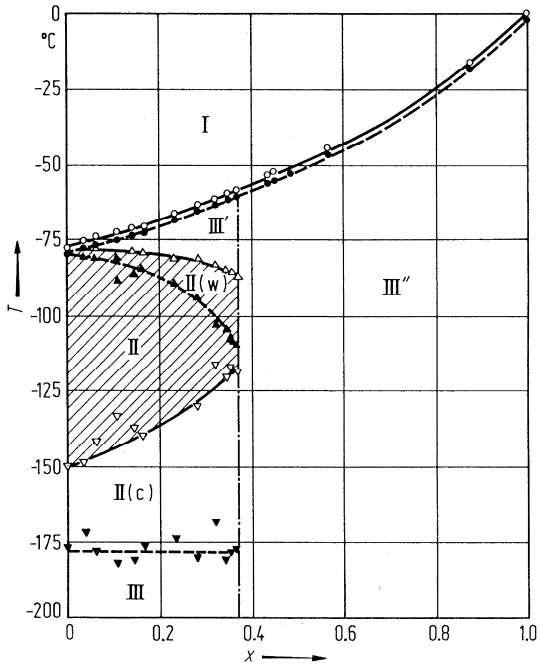

Fig. 31A-2-001. $Na(H_{1-x}D_x)_3(SeO_3)_2$. Phase diagram [70Mik]. Determined by anomalies in the linear thermal expansion along the *b* axis. Solid lines: phase boundaries observed on heating, dashed lines: on cooling; II(w) stands for phase II on warming, II(c) for phase II on cooling, etc. A similar phase diagram has been obtained by dielectric measurement [72Shu]. See also [68Zhe]. The hatched area shows the region of phase II(w), i.e. phase II observed on the warming.

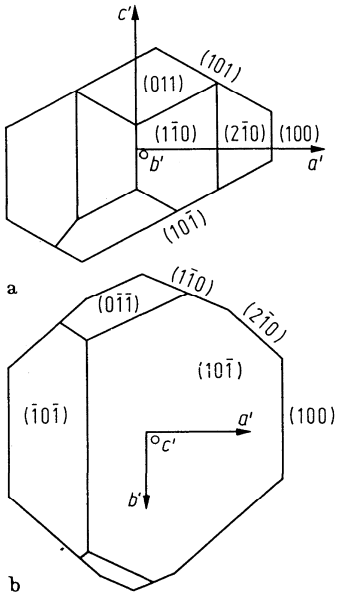

Fig. 31A-2-002. $NaD_3(SeO_3)_2$. Crystal form [69Sod]. (**a**) Viewed along the *b′* axis, (**b**) viewed along the *c′* axis.

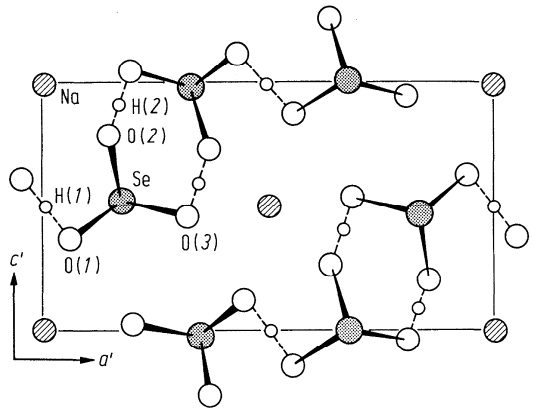

Fig. 31A-2-003. $NaH_3(SeO_3)_2$. Crystal structure of phase I [70Kap]. Viewed along the b' axis.

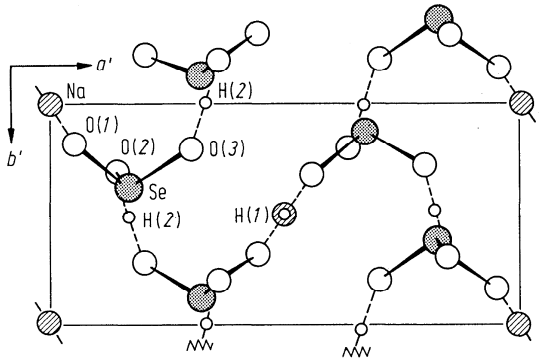

Fig. 31A-2-004. $NaH_3(SeO_3)_2$. Crystal structure of phase I [70Kap]. Viewed along the c' axis.

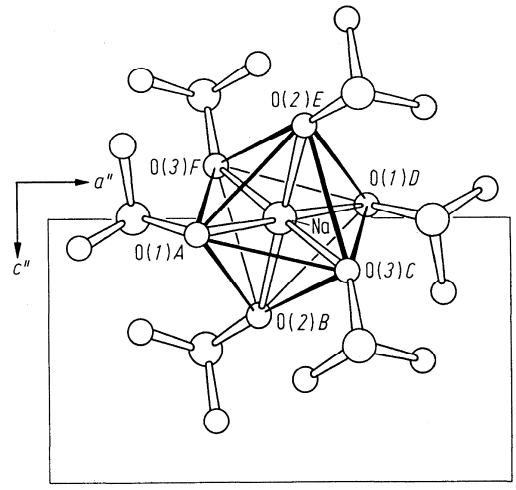

Fig. 31A-2-005. $NaH_3(SeO_3)_2$. Crystal structure of phase I [68Vij]. Environment of the sodium ions, as viewed along the b'' axis.

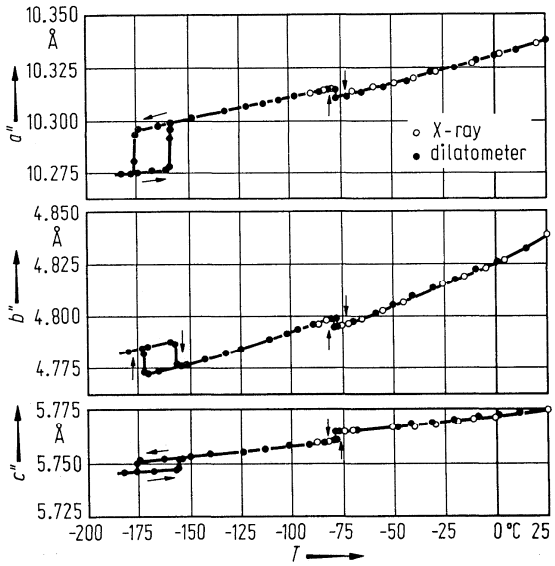

Fig. 31A-2-006. $NaH_3(SeO_3)_2$. a'', b'', c'' vs. T [70Mik].

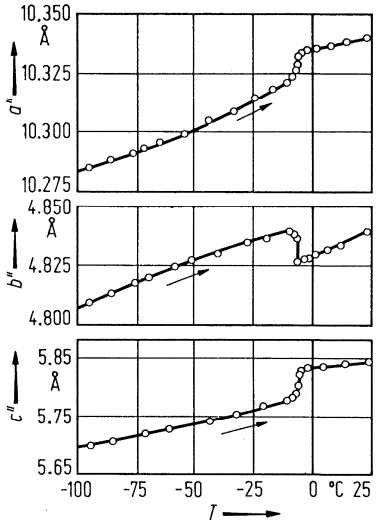

Fig. 31A-2-007. $NaD_3(SeO_3)_2$. a'', b'', c'' vs. T [70Mik].

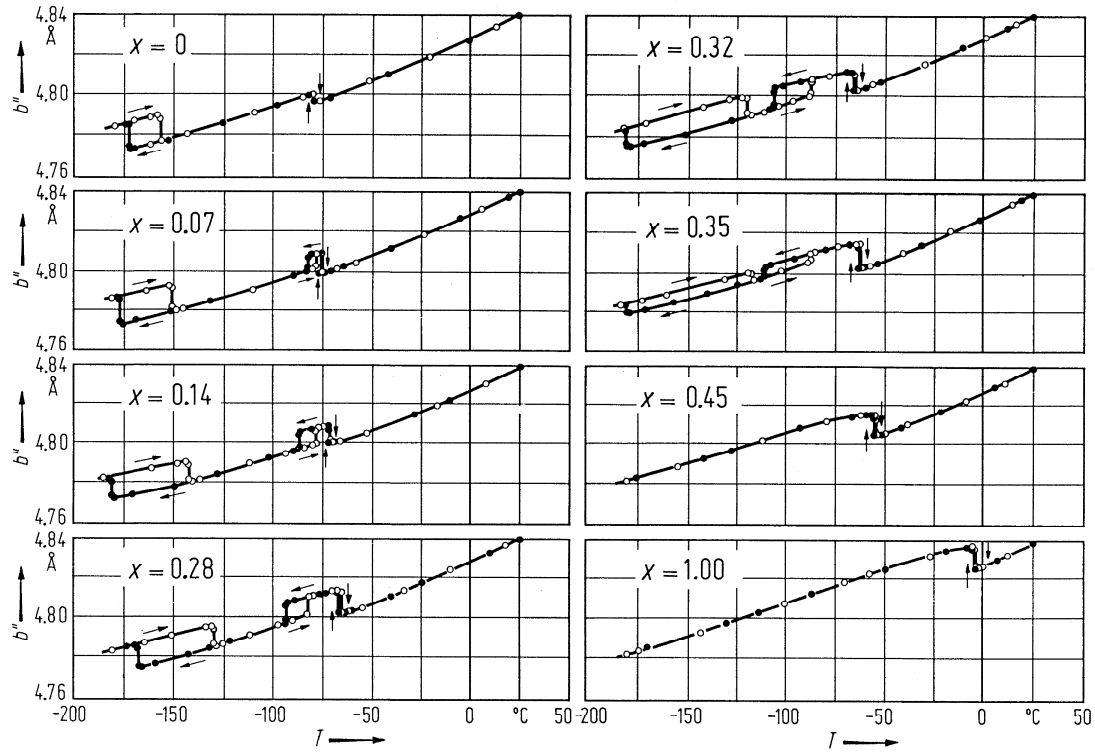

Fig. 31A-2-008. $Na(H_{1-x}D_x)_3(SeO_3)_2$. b'' vs. T [70Mik]. Parameter: x.

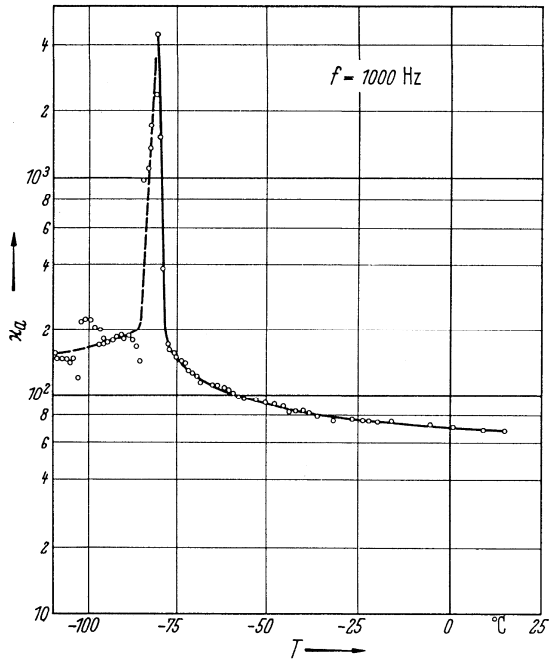

Fig. 31A-2-009. $NaH_3(SeO_3)_2$. κ_a vs. T [65Bli].

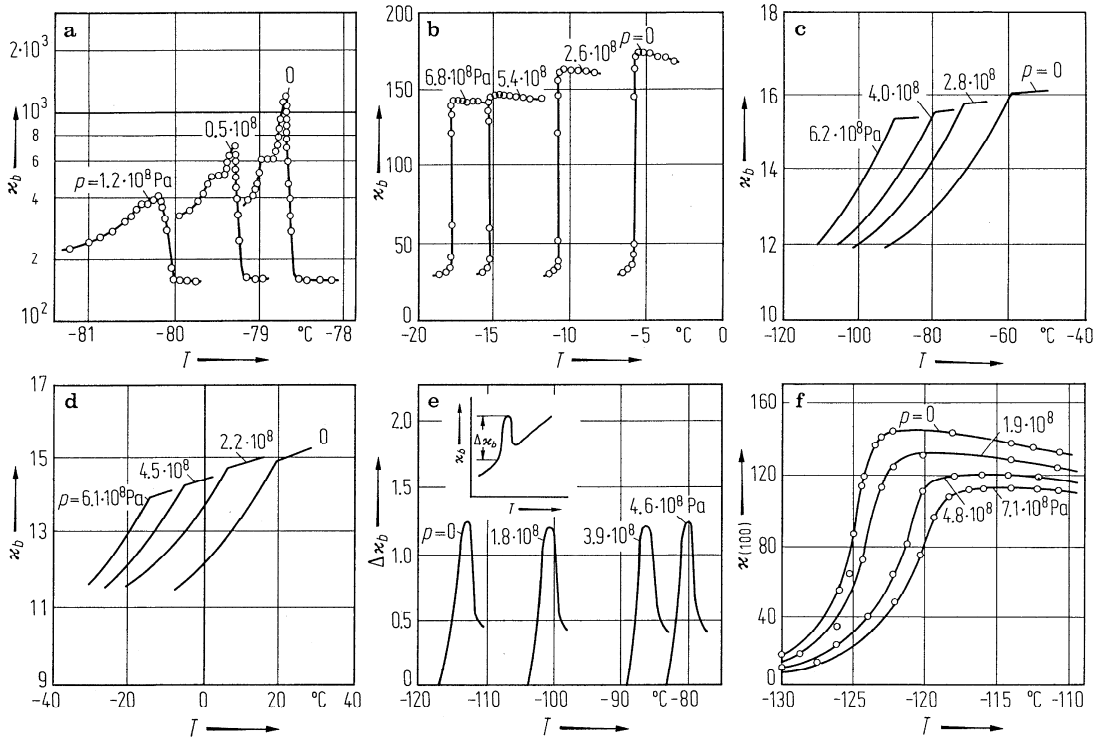

Fig. 31A-2-010. $XH_3(SeO_3)_2$, $XD_3(SeO_3)_2$, X = Na, K, Rb, Cs. κ vs. T [71Shi]. Parameter: p. (**a**) $NaH_3(SeO_3)_2$; (**b**) $NaD_3(SeO_3)_2$; (**c**) $KH_3(SeO_3)_2$; (**d**) $KD_3(SeO_3)_2$; (**e**) $RbH_3(SeO_3)_2$; (**f**) $CsH_3(SeO_3)_2$. $\kappa_{(100)}$: dielectric constant perpendicular to the (100) plane. κ: low frequency dielectric constant.

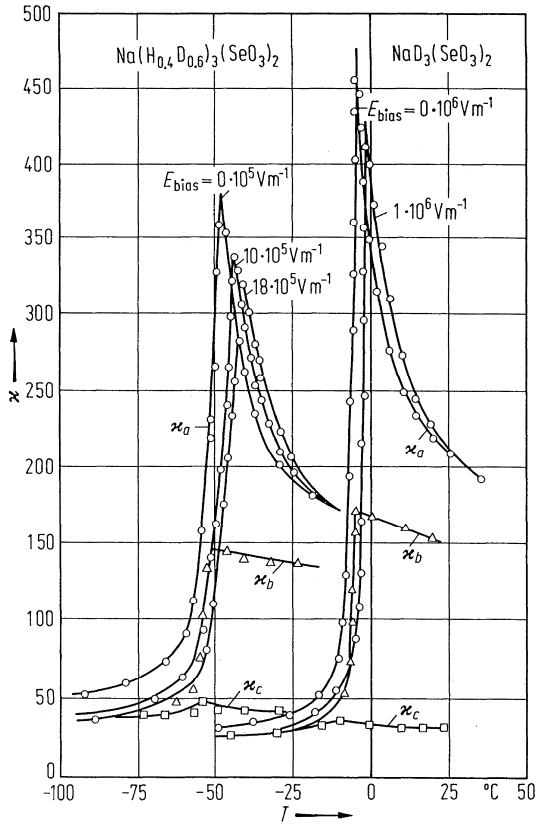

Fig. 31A-2-011. $NaD_3(SeO_3)_2$, $Na(H_{0.4}D_{0.6})_3(SeO_3)_2$. κ vs. T [69Shu]. f = 800 Hz. Parameter: E_{bias}.

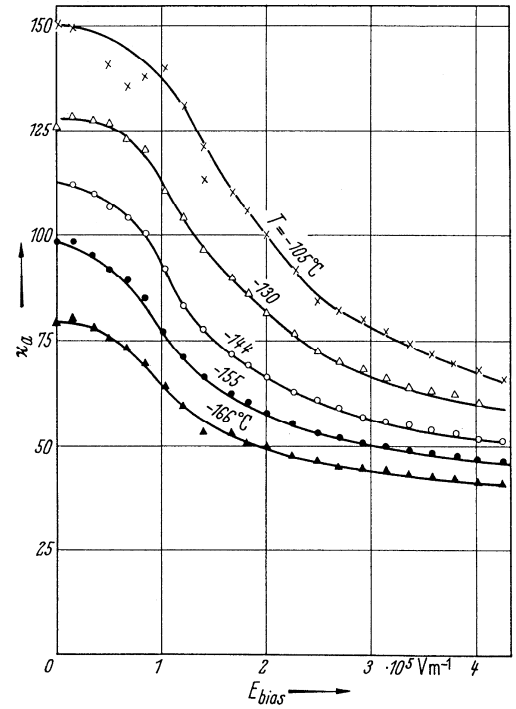

Fig. 31A-2-012. $NaH_3(SeO_3)_2$. κ_a vs. E_{bias} [65Bli]. f = 200 kHz. Parameter: T.

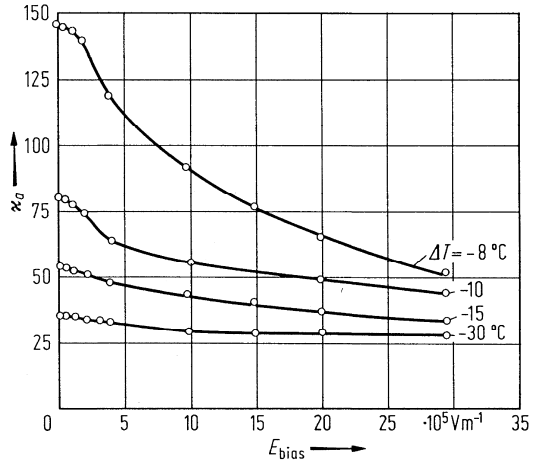

Fig. 31A-2-013. $NaD_3(SeO_3)_2$. κ_a vs. E_{bias} [69Shu]. f = 800 Hz. Parameter: $\Delta T = T - \Theta_{II-I}$.

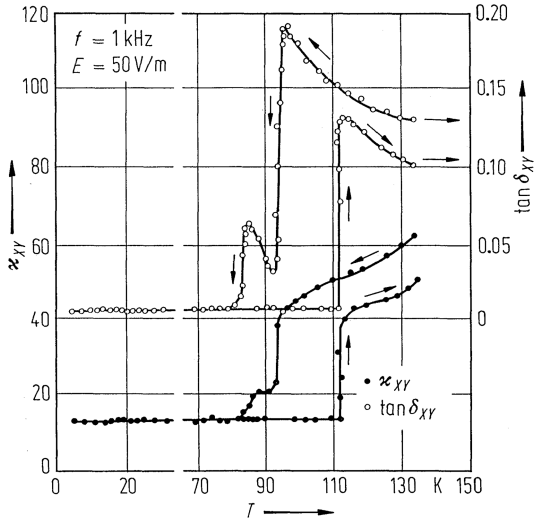

Fig. 31A-2-014. $NaH_3(SeO_3)_2$. κ_{XY}, $\tan\delta_{XY}$ vs. T [86Bon]. κ_{XY}, $\tan\delta_{XY}$: dielectric constant and dielectric loss tangent of XY-cut specimen. $\boldsymbol{Y} \parallel \boldsymbol{b}$ and $\boldsymbol{X} \parallel$ bisector of the acute angle between optical axes at RT.

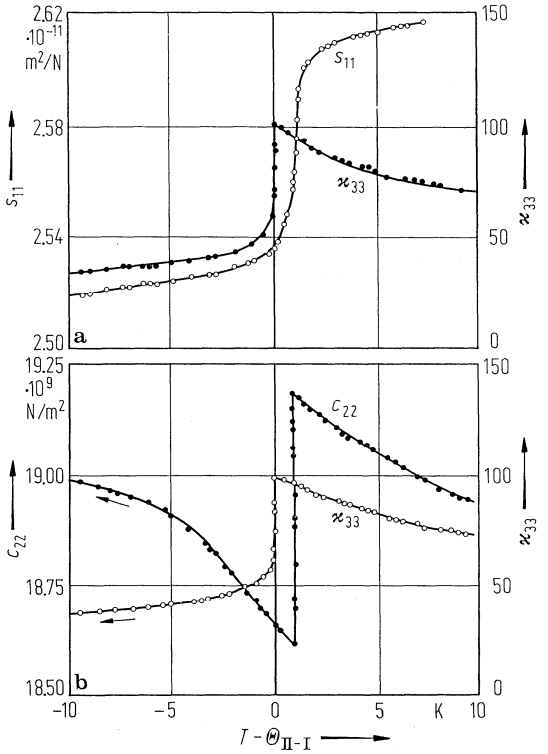

Fig. 31A-2-015. $NaH_3(SeO_3)_2$. (**a**) s_{11}, κ_{33} vs. $T - \Theta_{I-I}$ [86Jan]. s_{11}: elastic compliance measured by resonance method. (**b**) c_{22}, κ_{33} vs. $T - \Theta_{I-I}$. c_{22}: elastic stiffness measured by ultrasonic method. Cartesian axes Y and Z are along the crystallographic b and a axes, respectively. The X axis is orthogonal to the Y and Z axes.

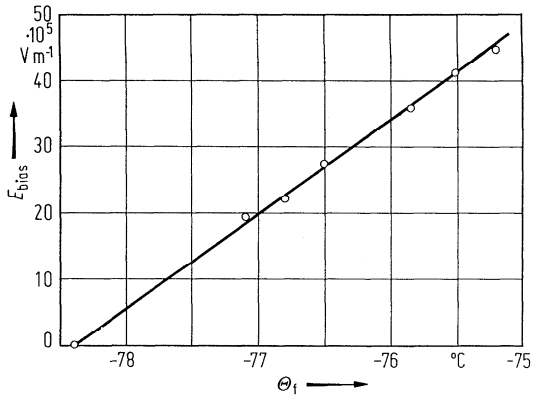

Fig. 31A-2-016. $NaH_3(SeO_3)_2$. Θ_f vs. E_{bias} [70Bli]. $E_{bias} \| a$.

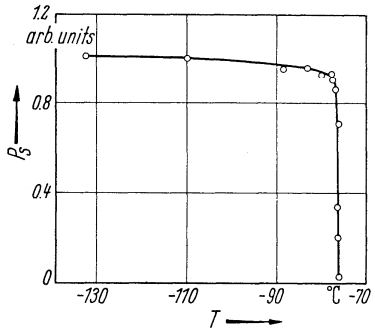

Fig. 31A-2-017. $NaH_3(SeO_3)_2$. P_s vs. T [65Bli].

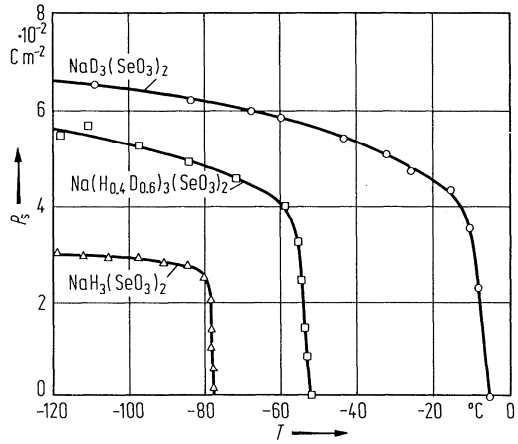

Fig. 31A-2-018. $Na(H_{1-x}D_x)_3(SeO_3)_2$. P_s vs. T [69Shu]. P_s is measured along the *a* axis.

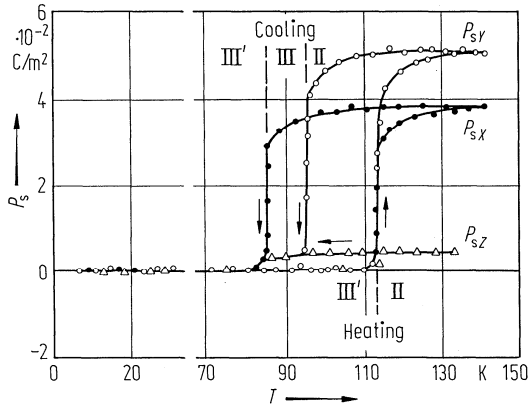

Fig. 31A-2-019. $NaH_3(SeO_3)_2$. P_{sX}, P_{sY}, P_{sZ} vs. T [86Bon]. P_{sX}, P_{sY}, P_{sZ}: components of spontaneous polarization along *X*, *Y*, *Z* directions, respectively. $\boldsymbol{Y} \parallel \boldsymbol{b}$ and $\boldsymbol{X} \parallel$ bisector of the acute angle between optical axes at RT.

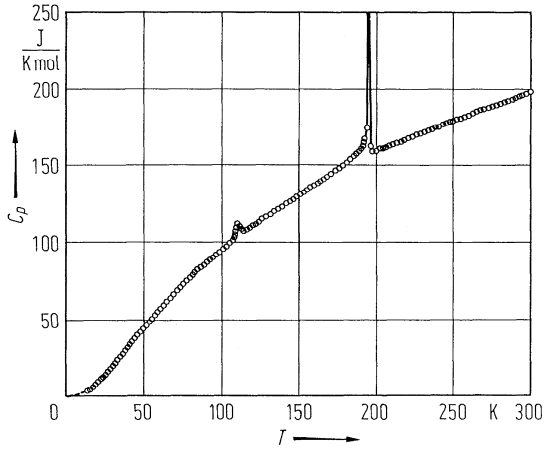

Fig. 31A-2-020. $NaH_3(SeO_3)_2$. C_p vs. T [76Mat]. C_p: molar heat capacity at constant pressure.

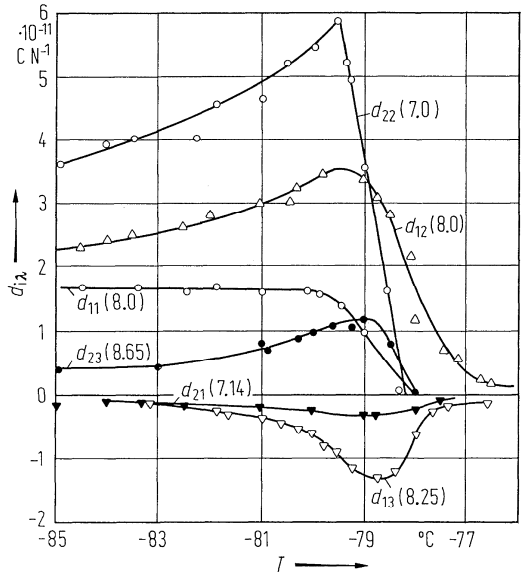

Fig. 31A-2-021. $NaH_3(SeO_3)_2$. $d_{i\lambda}$ vs. T [75Sch]. Figures in the parentheses indicate biasing fields in 10^5 V m^{-1}.

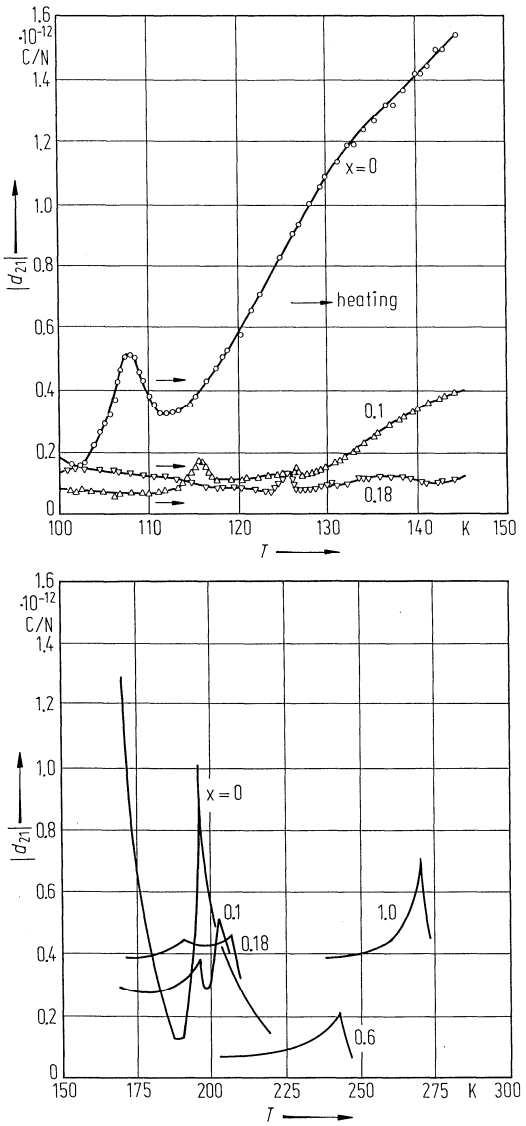

Fig. 31A-2-022. $Na(H_{1-x}D_x)_3(SeO_3)_2$. $|d_{21}|$ vs. T [86Sor]. d_{21}: piezoelectric constant. Parameter: x.

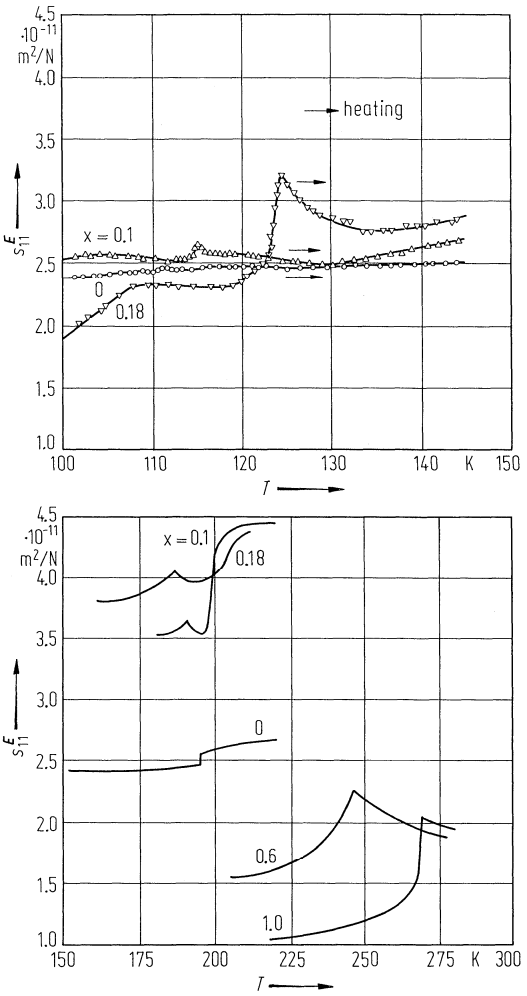

Fig. 31A-2-023. $Na(H_{1-x}D_x)_3(SeO_3)_2$. s_{11}^E vs. T [86Sor]. Parameter: deuterium concentration x. A dc electric field $E_2 = 7 \cdot 10^2$ kV/m was applied.

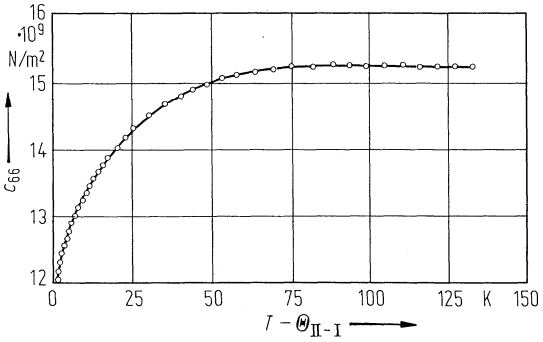

Fig. 31A-2-024. $NaH_3(SeO_3)_2$. c_{66} vs. $T - \Theta_{II-I}$ [80Sor]. $f = 20$ MHz.

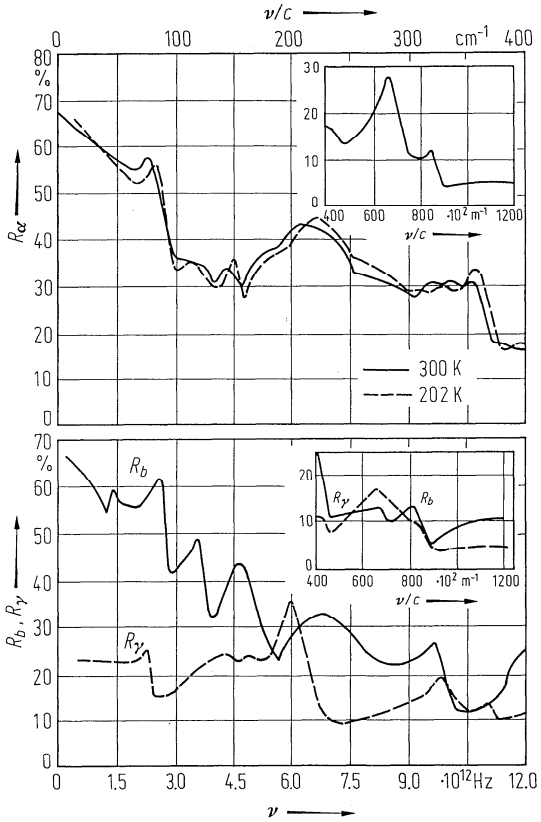

Fig. 31A-2-025. $NaH_3(SeO_3)_2$. R_α, R_b, R_γ vs. ν [70Sug]. R_b: reflectivity for the light with polarization parallel to the *b* axis. R_α, R_γ: parallel to two extinction directions in the *ac* plane.

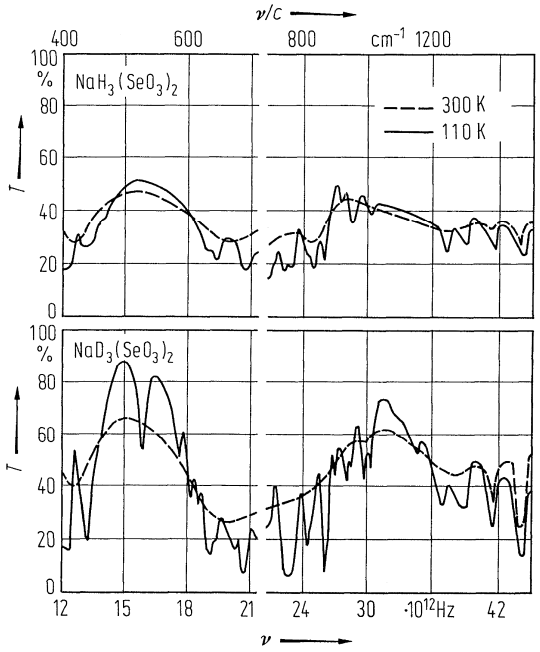

Fig. 31A-2-026. $NaH_3(SeO_3)_2$, $NaD_3(SeO_3)_2$. T vs. ν [73Ach]. T: transmission of the infrared radiation. The deuterium content is estimated to be more than 80%.

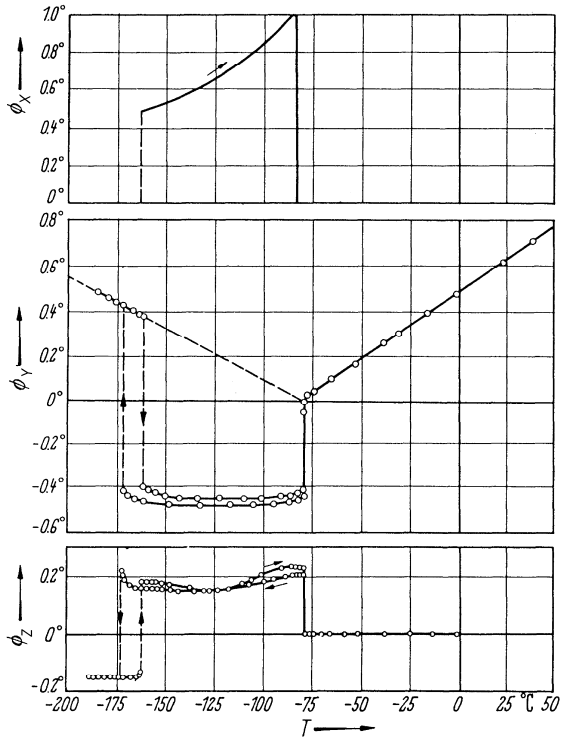

Fig. 31A-2-027. $NaH_3(SeO_3)_2$. ϕ_X, ϕ_Y, ϕ_Z vs. T [67Shu]. ϕ_X, ϕ_Y, ϕ_Z: rotational angles of indicatrix around X, Y and Z.

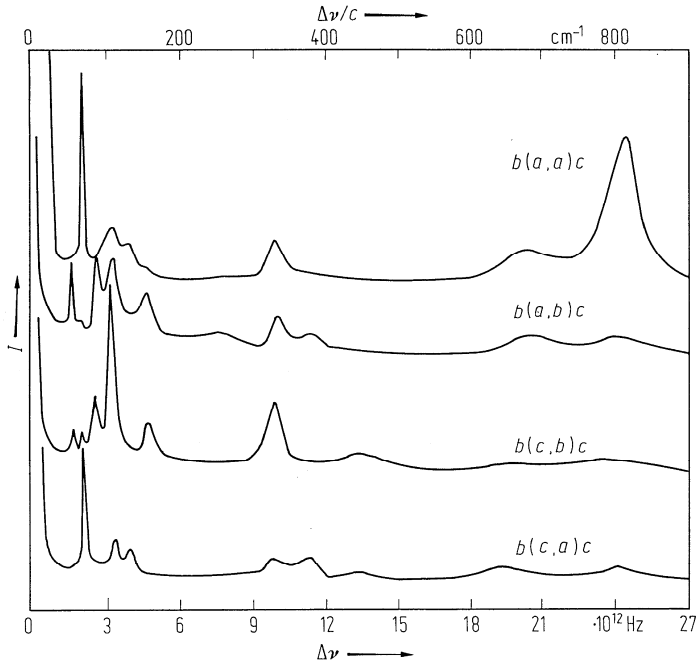

Fig. 31A-2-028. $NaH_3(SeO_3)_2$. I vs. $\Delta\nu$ [73Ach]. I: Raman scattering intensity at room temperature for various scattering geometries.

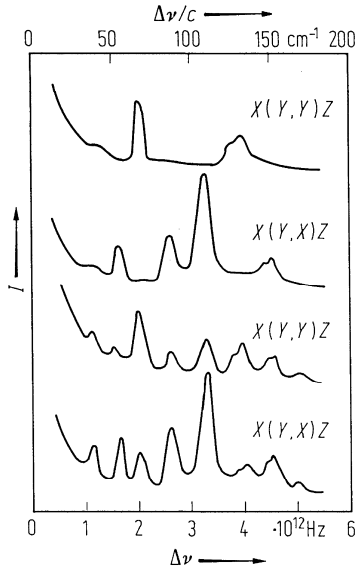

Fig. 31A-2-029. $NaH_3(SeO_3)_2$. I vs. $\Delta\nu$ near Θ_{II-I} [75Sha]. I: Raman scattering intensity for various scattering geometries. Upper two spectra are for $T > \Theta_{II-I}$, and the lower two are for $T < \Theta_{II-I}$.

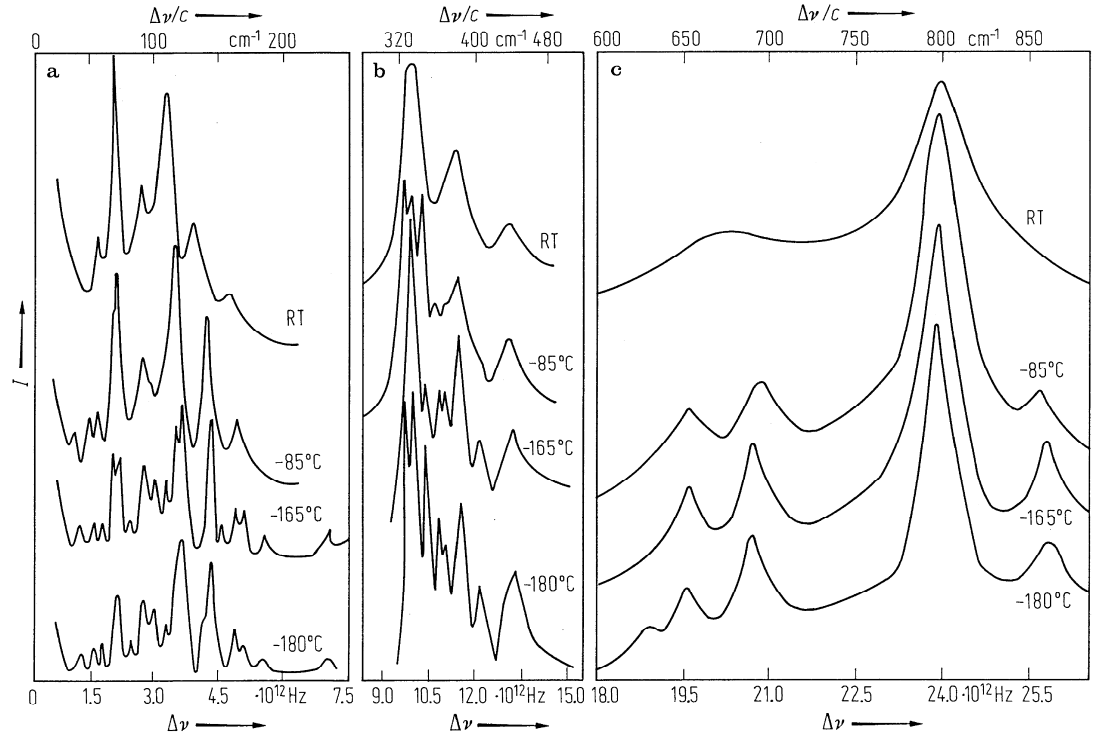

Fig. 31A-2-030. $Na(H_{0.9}D_{0.1})_3(SeO_3)_2$. I vs. $\Delta\nu$ [73Tor]. I: Raman scattering intensity for various temperatures. The sample was a pellet and polarization geometry was not specified.

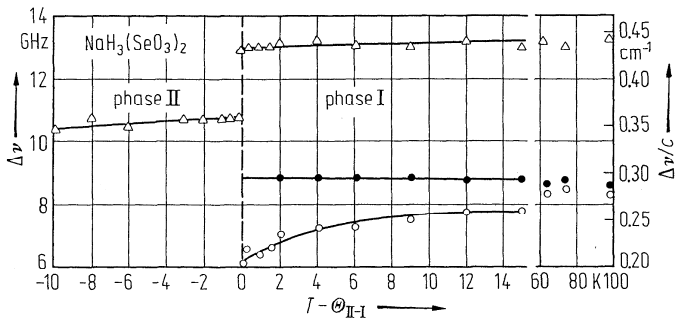

Fig. 31A-2-031. $NaH_3(SeO_3)_2$. $\Delta\nu$ vs. $T - \Theta_{II-I}$ [76Lav]. $\Delta\nu$: Brillouin shift. Wave vector || [100]. Open circles: transverse mode; full circles: quasi-transverse mode; open triangles: quasi-longitudinal mode.

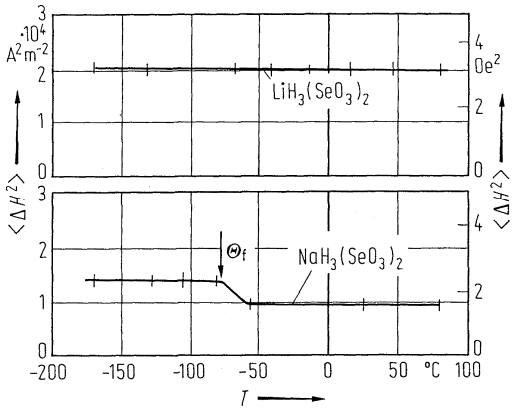

Fig. 31A-2-032. $NaH_3(SeO_3)_2$, $LiH_3(SeO_3)_2$. $\langle\Delta H^2\rangle$ vs. T [61Bli]. $\langle\Delta H^2\rangle$: second moment of proton.

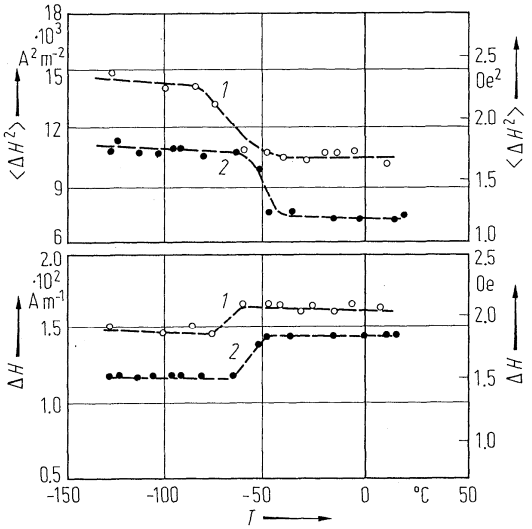

Fig. 31A-2-033. $Na(H_xD_{1-x})_3(SeO_3)_2$. $\langle\Delta H^2\rangle$, ΔH vs. T [67Gav]. $\langle\Delta H^2\rangle$: second moment of proton, ΔH: half width of proton. Curve *1*: x = 1, curve *2*: x = 0.58.

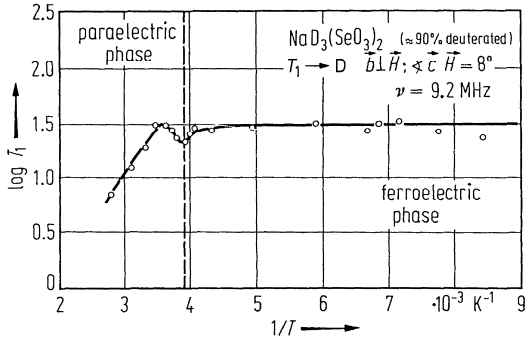

Fig. 31A-2-034. $NaD_3(SeO_3)_2$. log T_1 vs. 1/T [68Bli]. T_1: deuteron spin-lattice relaxation time [in s].

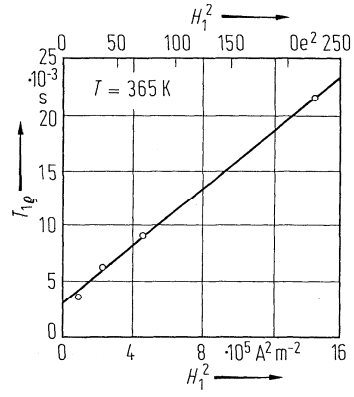

Fig. 31A-2-035. $NaH_3(SeO_3)_2$. $T_{1\rho}$ vs. H_1^2 [71Bli]. $T_{1\rho}$: proton spin-lattice relaxation time in the rotating frame; H_1: radio frequency magnetic field strength.

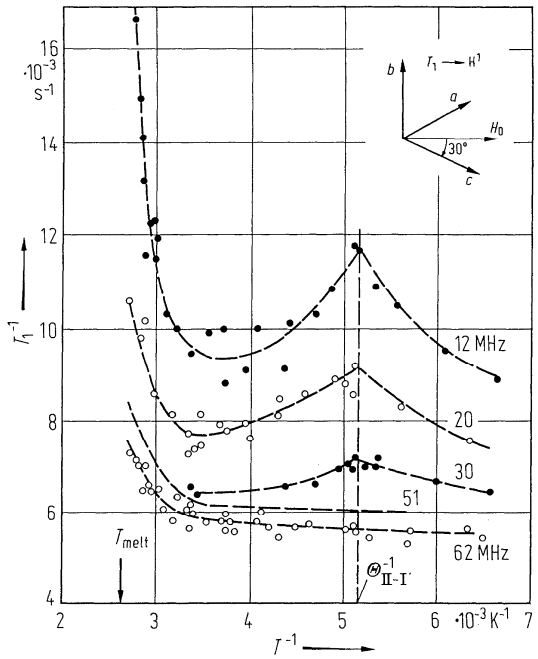

Fig. 31A-2-036. $NaH_3(SeO_3)_2$. T_1^{-1} vs. T^{-1} [74Adr]. T_1^{-1}: inverse of the proton spin-lattice relaxation time. See also [71Khi, 76Mal].

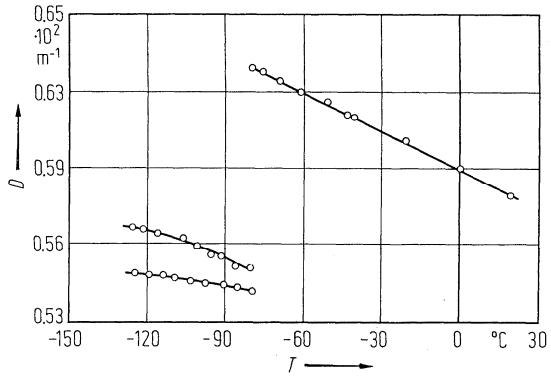

Fig. 31A-2-037. $NaH_3(SeO_3)_2$. *D* vs. *T* [77Mal]. *D*: crystalline field parameter of Cr^{3+} substituted for Na^+.

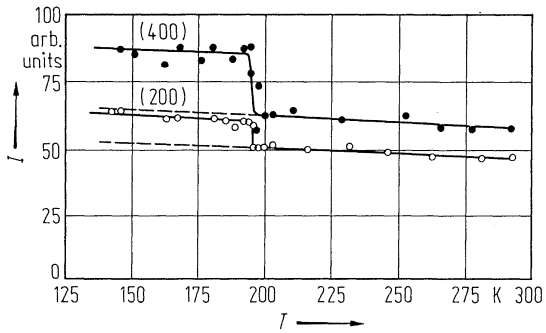

Fig. 31A-2-038. $NaH_3(SeO_3)_2$. $I_{(200)}$, $I_{(400)}$ vs. *T* [73Mik]. *I*: integrated intensity of X-ray Bragg reflection. The coordinates refer to the *a*′, *b*′, *c*′ axial system.

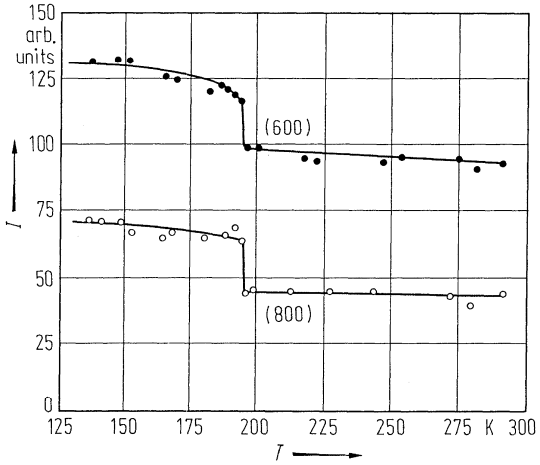

Fig. 31A-2-039. $NaH_3(SeO_3)_2$. $I_{(600)}$, $I_{(800)}$ vs. *T* [73Mik]. *I*: integrated intensity of X-ray Bragg reflection. The coordinates refer to the *a*′, *b*′, *c*′ axial system.

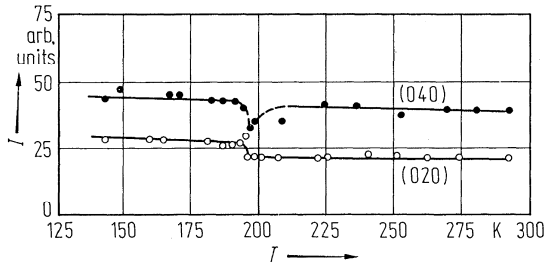

Fig. 31A-2-040. $NaH_3(SeO_3)_2$. $I_{(040)}$, $I_{(020)}$ vs. T [73Mik]. I: integrated intensity of X-ray Bragg reflection. The coordinates refer to the a', b', c' axial system.

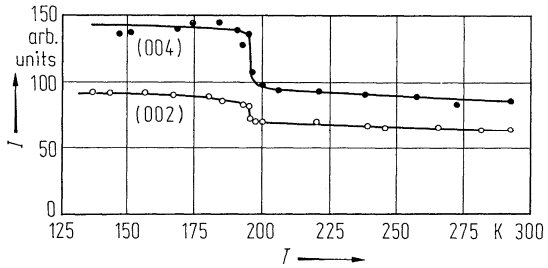

Fig. 31A-2-041. $NaH_3(SeO_3)_2$. $I_{(004)}$, $I_{(002)}$ vs. T [73Mik]. I: integrated intensity of X-ray Bragg reflection. The coordinates refer to the a', b', c' axial system.

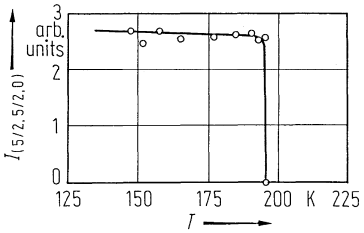

Fig. 31A-2-042. $NaH_3(SeO_3)_2$. $I_{(5/2,5/2,0)}$ vs. T [73Mik]. I: integrated intensity of X-ray superlattice reflection. The coordinates refer to the a', b', c' axial system.

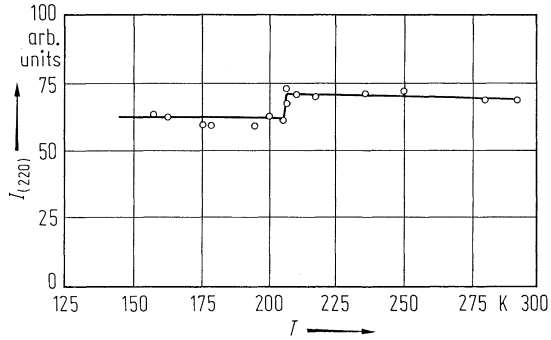

Fig. 31A-2-043. $NaH_3(SeO_3)_2$. $I_{(220)}$ vs. T [73Mik]. I: integrated intensity of X-ray Bragg reflection. The coordinates refer to the a', b', c' axial system.